Article

MMS

Mathematics and Mechanics of Solids
1–18

DOI: 10.1177/1081286519877684
journals.sagepub.com/home/mms
SAGE

Surface effects of network materials based on strain gradient homogenized media

Y Rahali
IPEIB, Université de Carthage, Zarzouna (Bizerte), Tunisia

VA Eremeyev
Gdansk University of Technology, Poland

JF Ganghoffer
LEM3 Université de Lorraine, CNRS, Metz, France

Received 22 May 2019; accepted 2 September 2019

Abstract
The asymptotic homogenization of periodic network materials modeled as beam networks is pursued in this contribution, accounting for surface effects arising from the presence of a thin coating on the surface of the structural beam elements of the network. Cauchy and second gradient effective continua are considered and enhanced by the consideration of surface effects. The asymptotic homogenization technique is here extended to account for the additional surface properties, which emerge in the asymptotic expansion of the effective stress and hyperstress tensors versus the small scale parameters and the additional small parameters related to surface effects. Based on the elaboration of small dimensionless parameters of geometrical or mechanical nature reflecting the different length scales, we construct different models in which the importance of surface effects is dictated by specific choice of the scaling relations between the introduced small parameters. The effective moduli reflect the introduced surface properties. We show in particular that surface effects may become dominant for specific choices of the scaling laws of the introduced small parameters. Examples of networks are given for each class of the considered effective constitutive models to illustrate the proposed general framework.

Keywords
Homogenization, second gradient, coupling energy, surface effects

1. Introduction

Classical homogenization of network materials with a discrete topology towards an effective Cauchy continuum has been an active research field since many years, and several methods have been developed over the last two decades [1–7]. Nevertheless this technique encounters limitations when the wavelength of the loading or deformation field becomes comparable with the typical microstructure size. More notably size effects could not be captured by standard elasticity theory [8]. The main motivation that makes

Corresponding author:
JF Ganghoffer, LEM3 Université de Lorraine, CNRS, 7, rue Félix Savart, BP 15082, 57073 Metz Cedex 03, France.
Email: jean-francois.Ganghoffer@univ-lorraine.fr

scientists in 1960s–1970s develop the non-classical continuum mechanics theories from a mathematical point of view and the objective of homogenization towards generalized continua is to extend the range of validity of the continuum approach beyond the strict assumption of the scale separation [9]. As mentioned by Forest [10], the method to be used must be able to account for the effect of the morphology and distribution of phases on the material response and to predict scale effects. The general class of so-called microstructured models or higher order continuum models allows a description of the kinematics of the microstructure by using an additional tensor in the displacement field or additional intrinsic parameters and internal length scales to correlate the microstructure with its macro-modeling via suitably introduced macro-fields [11,12]. Higher order continuum theories can be traced back to the works of Cosserat and Cosserat [13], Toupin [14], and Mindlin [15,16], and have been generalized and properly formulated by Germain [17] and Sedov [18] using the virtual power method.

Some higher-order micro-continuum theories have been developed to account for the microstructure effects by introducing additional degrees of freedom (such as the Cosserat medium [19] and the micromorphic medium [20]) or additional higher-order gradients such as the second gradient continuum [14,21] and material constants to the conventional ones [15,16,22–33]. Strain localization zones are clearly observed in experimental tests [34] and it is well known that they cannot be modeled with classical (without an internal length parameter) continuum mechanics models. Several authors have turned their attention towards the development of homogenization procedures with the ability to account for the heterogeneous nature of the material at the micro level using a second-order macroscopic constitutive law [35,36]; works in this direction consider both linear elastic materials and nonlinear materials. Higher-order homogenization schemes have been built for architectured materials in both the linear and nonlinear regimes in the work of Trinh et al. [9]. The recent work of El Jarroudi [37] deals with the homogenization of nonlinear elastic material in contact with a set of more rigid nonlinear elastic fibers disposed periodically within the structure. The authors choose to work with the second gradient model developed by Chambon et al. [38–40]. This model can be seen as a particular case of a higher order continuum and has been mainly used to regularize problems involving strain localization in soils.

In the present work, we construct an effective second order gradient continuum for repetitive network materials based on beam-like structural elements and including surface effects due to the presence of a thin coating on the beam structural elements. The discrete asymptotic expansion method (DH method in short) dedicated to the construction of effective continuum substitution media for repetitive networks is extended up to the second-order gradient of the displacement field to derive the constitutive law expressing the first-order Cauchy stress and the second-order hyperstress versus their conjugated kinematic variables. The developed framework based on the principle of virtual power and the homogenization of beam lattices allows incorporating local microstructural effects via the consideration of the second-order displacement gradient. The chief advantage of the DH method exposed in this contribution is the ease of geometrical modeling and numerical implementation, especially in comparison to computations based on the finite element (FE) method. In fact a high accuracy of local stress peak requires fine meshes resulting in long computation times. In addition, FE computations result in a huge number of degrees of freedom effectively increasing the size of stiffness matrices. The DH method involves comparatively a much smaller number of degrees of freedom since the beam degrees of freedom within the unit cell are only defined at its extremity nodes, whereas FE computations requires meshing all entities as three-dimensional (3D) solids. The low cost computations allow computing in a quite efficient manner the effective anisotropic mechanical properties of two-dimensional (2D) and 3D repetitive network materials. Furthermore, as will be apparent in the selected examples, the homogenization method is able to deliver in many cases closed-form expressions of the effective first- and second-order moduli.

The aim of the paper is to evaluate the effective anisotropic material properties of nanostructured network materials at the mesoscale of an effective continuum considering surface/interface properties. It is well established that unusual and novel properties of nanomaterials emerge from their surface/interfacial properties. One well-known consequence of surface properties is the so-called size effect, i.e. the dependence of the effective mechanical properties on the size of the considered specimen [41–45]. The presence of a coating in these surface metamaterials dramatically changes the surface physical properties of the material and in turn all the material properties. Let us briefly discuss the mathematical models and methods used in surface-related mechanics. The analysis of surface phenomena traces back to the pioneer

works of Laplace [46,47], Young [48], and Poisson [49] who introduced surface tension for fluids and formulated the corresponding boundary-value problems. Gibbs generalized later on the notion of surface tension in the case of solids [50]. For the recent state of the art in the theory of capillarity one can refer to De Gennes et al. [51] and Rowlinson and Widom [52].

A model of surface elasticity for elastic solids undergoing large deformations was proposed by Gurtin and Murdoch [53,54], relying on the physical point of view of a nonlinear solid with an elastic membrane attached on its surface. The stress resultant tensor within the membrane receives the interpretation of surface stresses in the context of the Gurtin–Murdoch model. The Gurtin–Murdoch model found many applications in micro- and nanomechanics; it predicts the size effects observed for nanosized materials [55], so in situations where the effective material properties deviate from the ones of the bulk corresponding materials. This model was generalized [56,57] to account for the bending stiffness of the thin film or coating attached onto the surface of the bulk material. The different models developed in the literature that incorporate surface effects involve enhanced constitutive equations including a description of the surface behavior, whereby the introduced surface stress tensor depends on the surface strain measure. More general surface models beyond the Gurtin–Murdoch model have been developed in the literature [58–66], like for instance the model of a Cosserat surface for material interfaces [67]. These extended models include additional material parameters that should be determined, and that do influence the actual properties of materials [68–74]. It was shown in particular that the presence of surface stresses leads to the stiffening of the material in the context of the linear theory of elasticity [75–81].

The objectives of this contribution are as follows: we shall derive asymptotic expansions of the classical Cauchy stress and the second gradient tensors versus the introduced small scale parameters for network materials, incorporating surface effects. The importance of the surface effects will be assessed using different scaling laws of the small parameters inherent to surface effects versus the size parameter, defined as the ratio of the identified network unit cell to a macroscopic network length; based on this analysis, we shall derive conditions under which surface effects are important.

The outline of this contribution is as follows. In Section 2, we provide a clarification of the models developed in this work and we describe the homogenization process leading to the identification of the effective second-order continuum for 2D structures accounting for surface effects, based on a simplified Euler–Bernoulli scheme. A 2D example illustrating the proposed second order homogenization scheme is presented in Section 3. Finally, we conclude in Section 4 by a summary of the main developments and perspectives for future developments.

Regarding notation, vectors and tensors are denoted with boldface symbols.

2. Discrete homogenization towards a second gradient effective continuum using simplified Euler–Bernoulli scheme

The general idea at the root of the discrete homogenization method is the periodic repetition of an elementary cell made of beams connected at nodes to define an infinite network. Consider a finite 2D (surface) or 3D structure, parameterized by a small parameter ε, defined as the ratio between characteristic lengths of the lattice unit cell to a characteristic length of the entire network, scalar quantity L (Figure 1). For a large enough lattices, the ratio of the beam length, the scalar $l^{\varepsilon b}$, to a macroscopic

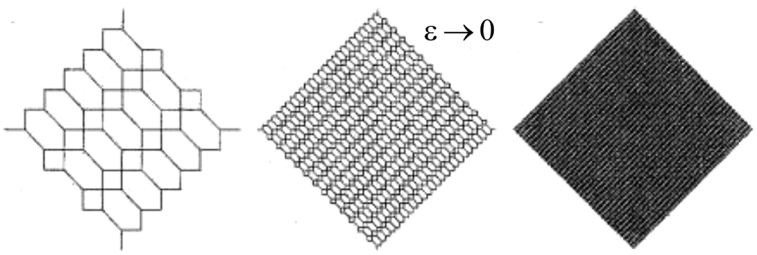

Figure 1. Set of repetitive lattices parameterized by a small parameter ε

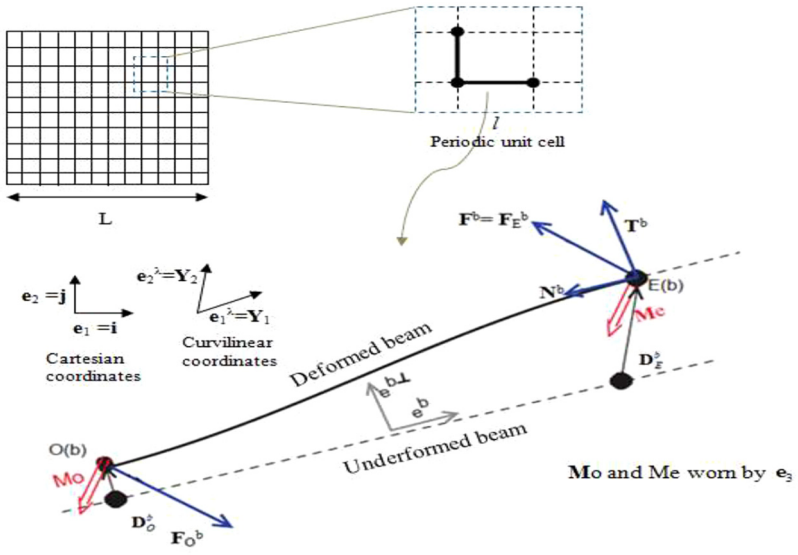

Figure 2. Kinematic and static beam parameters.

lattice length constitutes a small parameter versus which all geometrical and kinematic variables will be expanded, hence $l^{\varepsilon b} = \varepsilon L$.

Maintaining the reference area or volume fixed one considers the limit situation of a continuous density of unit cells obtained when the small parameter tends to zero. In this limit, a continuum, equivalent in a certain sense to the initial lattice is obtained. In order to obtain this limit behavior, one does mathematically study the equilibrium of the lattice and the dependence of the governing equations versus the introduced small parameter. Asymptotic expansions of the nodal position, tensions and external forces are written and inserted in the equilibrium equations, preferably expressed in weak form. Taylor series expansion of the displacements and possibly rotational degrees of freedom are next inserted into these equilibrium equations. The discrete sums are finally converted in the limit of a continuous density of beams into Riemann integrals, thereby highlighting continuous stress and strain measures. We mentally isolate a beam within the repetitive network (Figure 2), with extremity nodes O and E and length l^{ε}_b, with ε the ratio of the elementary unit cell l to the macroscopic network size L, illustrated in Figure 2; the small parameter ε tends to 0, so that the asymptotic expansion of the beam length can be written as $l^{\varepsilon}_b = \varepsilon L$.

Each beam works in tension-compression under the action of normal forces N_O and N_E applied to the extremity nodes and in flexion under the action of the transverse forces T_O, T_E and the moments M_O and M_E, as illustrated in Figure 2.

The following small parameters are introduced that will prove useful in order to quantify the importance of surface effects:

- $\varepsilon = l^b/L$ the ratio of beam length to a macroscopic characteristic length of the network;
- $\varepsilon_M = l_s/l^b$ with $l_s = 2E_s/E$ the ratio of (twice) the surface modulus of the coating to the bulk modulus of the beam material, called the characteristic length parameter [82];
- $\varepsilon_s = h/l^b$ the ratio of the thickness coating to the beam length.

We can make a further assumption in terms of the power relation between parameters l^b and h:

- $\varepsilon_s = \varepsilon^\beta$, introducing therein a new exponent β.

We consider that the slenderness ratio of the beam, parameter $\eta = t/l^b \cong t_c/l^b$, is finite.

The total beam thickness is the sum of the thickness of the core t_c and that of the coating, so that it holds the relation $t = t_c + h$. We further introduce the scaling exponent α to express $\varepsilon_M = \varepsilon^\alpha$. Based on

the introduced small parameters, the tensile modulus of the base material E_B is then enhanced by surface effects according to the relation [82]:

$$\tilde{E}_B = E_B\left(1+\frac{l_s}{t}\right) = E_B\left(1+\frac{l_s}{l^b}\frac{l^b}{t}\right) = E_B\left(1+\frac{\varepsilon_M}{\eta}\right) = E_B\left(1+\frac{\varepsilon^\alpha}{\eta}\right)$$

We consider a square section with area $\tilde{A} = t$, assuming a unit beam thickness. The modified tensile and flexural rigidities of the beam can now be expressed as

$$\begin{aligned}\tilde{k}_l &= \frac{\tilde{E}_B\tilde{A}}{l^b} = E_B\left(1+\frac{\varepsilon^\alpha}{\eta}\right)\frac{(t_c+h)}{l^b} \cong E_B\left(1+\frac{\varepsilon^\alpha}{\eta}\right)(\eta+\varepsilon_s) \equiv k_l + E_B(\varepsilon_s+\varepsilon^\alpha) + \frac{E_B}{\eta}\varepsilon_s\varepsilon^\alpha \\ &= k_l + E_B\left(\varepsilon^\beta+\varepsilon^\alpha\right) + \frac{E_B}{\eta}\varepsilon^{\alpha+\beta}\end{aligned} \tag{1}$$

$$\begin{aligned}\tilde{k}_f &= \frac{12\tilde{E}_B\tilde{I}}{\left(l^b\right)^3} = E_B\left(1+\frac{\varepsilon^\alpha}{\eta}\right)\left(\eta+\varepsilon_\beta\right)^3 \cong E_B\left(\eta^3+3\varepsilon_\beta\eta^2+\varepsilon^\alpha\eta^2+3\eta\varepsilon_\beta\varepsilon^\alpha\right) \\ &= k_f + 3\eta^2E_B\varepsilon_\beta + E_B\eta^2\varepsilon^\alpha + 3E_B\eta\varepsilon_\beta\varepsilon^\alpha \\ &= k_f + 3\eta^2E_B\varepsilon^\beta + E_B\eta^2\varepsilon^\alpha + 3E_B\eta\varepsilon^{\alpha+\beta}\end{aligned} \tag{2}$$

$$\text{since } (\eta+\varepsilon_s)^3 \cong \eta^3(1+3\varepsilon_s/\eta) = \eta^3+3\varepsilon_s\eta^2 \Rightarrow \left(+1\frac{\varepsilon^\alpha}{\eta}\right)(+\eta\varepsilon_s)^3 \cong \left(\eta^3+3\varepsilon_s\eta^2\right)\left(1+\frac{\varepsilon^\alpha}{\eta}\right)$$
$$= \eta^3+3\varepsilon^\beta\eta^2+\varepsilon^\alpha\eta^2+3\eta\varepsilon^{\alpha+\beta}$$

$\tilde{I} = t^3/12$ is the quadratic moment of the considered beam. Note that η is finite, but $\varepsilon_s/\eta \to 0$. The first-order terms in previous relations defines successively the tensile and flexural rigidity in the absence of surface effects, quantities k_l and k_f.

This entails the following modified expression of forces and moments from beam theory [83] (it is in fact the simplified Bernoulli model, since rotations are not considered as independent kinematic variables) in vector form:

$$N_O^{\varepsilon b} = \tilde{k}_l^b\left(\mathbf{e}^b.\left(\mathbf{D}_O^\varepsilon - \mathbf{D}_E^\varepsilon\right)\right) = E_B\left(1+\frac{\varepsilon^\alpha}{\eta}\right)(\eta+\varepsilon^\beta)\left(\mathbf{e}^b.\left(\mathbf{D}_O^\varepsilon - \mathbf{D}_E^\varepsilon\right)\right) \tag{3}$$

$$N_E^{\varepsilon b} = -N_O^{\varepsilon b} \tag{4}$$

$$T_O^{\varepsilon b} = \tilde{k}_f^b\left(\mathbf{e}^{b\perp}.\left(\mathbf{D}_O^\varepsilon - \mathbf{D}_E^\varepsilon\right)\right) = E_B\left(1+\frac{\varepsilon^\alpha}{\eta}\right)(\eta+\varepsilon^\beta)^3\left(\mathbf{e}^{b\perp}.\left(\mathbf{D}_O^\varepsilon - \mathbf{D}_E^\varepsilon\right)\right) \tag{5}$$

$$T_E^{\varepsilon b} = -T_O^{\varepsilon b} \tag{6}$$

$$M_O^{\varepsilon b} = \frac{\tilde{k}_f l_b^\varepsilon}{6}\left(3.\mathbf{e}^{b\perp}.\left(\mathbf{D}_O^\varepsilon - \mathbf{D}_E^\varepsilon\right)\right).\mathbf{e}_3 = E_B\left(1+\frac{\varepsilon^\alpha}{\eta}\right)(\eta+\varepsilon^\beta)^3\frac{l_b^\varepsilon}{6}\left(3.\mathbf{e}^{b\perp}.\left(\mathbf{D}_O^\varepsilon - \mathbf{D}_E^\varepsilon\right)\right) \tag{7}$$

$$M_E^{\varepsilon b} = \frac{\tilde{k}_f l_b^\varepsilon}{6}\left(3.\mathbf{e}^{b\perp}.\left(\mathbf{D}_O^\varepsilon - \mathbf{D}_E^\varepsilon\right)\right).\mathbf{e}_3 = E_B\left(1+\frac{\varepsilon^\alpha}{\eta}\right)(\eta+\varepsilon^\beta)^3\frac{l_b^\varepsilon}{6}\left(3.\mathbf{e}^{b\perp}.\left(\mathbf{D}_O^\varepsilon - \mathbf{D}_E^\varepsilon\right)\right) \tag{8}$$

Vectors $\mathbf{D}_O^\varepsilon$ and $\mathbf{D}_E^\varepsilon$ are the displacements of the extremity nodes of the beam with components $\mathbf{D} = (U,V)_{(x,y)}$, $\mathbf{e}^b$ the unit director along the beam and $\mathbf{e}^{b\perp}$ the normal unit vector. The subscripts O and E refer to the origin and extremity nodes of the beam.

The steps for the determination of the Cauchy stress and hyperstress tensors of the second gradient continuum for this model are summarized in the sequel. We refer the reader to Rahali et al. [84] and Agrawal et al. [85] for more details related to the different steps of the method.

2.1. Homogenization steps

1. For each beam b, write the expressions of the normal N and transverse T forces and moments M exerted on the beam extremities, as summarized in equations (3)–(8).
2. Write the asymptotic expansion of geometrical and kinematic variables of each beam, in curvilinear coordinates denoted λ in the sequence:

- The beam length $l_b^\varepsilon = \varepsilon L_b$
- *The beam width* $t^{\varepsilon b} = \varepsilon t^b$
- The relative nodal displacement written as

$$(\mathbf{D}_O^\varepsilon - \mathbf{D}_E^\varepsilon) = \varepsilon\left(\mathbf{D}_1^O - \mathbf{D}_1^E - L_i\delta_{ib}\frac{\partial \mathbf{D}_o(\lambda^\varepsilon)}{\partial \lambda_i}\right) + \varepsilon^2\left(\mathbf{D}_2^O - \mathbf{D}_2^E - L_i\delta_{ib}\frac{\partial \mathbf{D}_1^E(\lambda^\varepsilon)}{\partial \lambda_i} - \frac{L_i^2\delta_{ib}^2}{2}\frac{\partial^2 \mathbf{D}_o(\lambda^\varepsilon)}{\partial \lambda_i^2}\right) \quad (9)$$

with δ_i the shift factor (equal to ± 1) for nodes belonging to a neighboring cell, and nil for nodes located inside the considered cell. The index $i \in \{1, 2\}$ indicating the considered axis e_1 or e_2 and the index b refer to the beam. One notices from previous expression that the relative displacement depends on both first and second gradients of the continuous macroscopic displacement, contributions $\partial \mathbf{D}_o(\lambda^\varepsilon)/\partial\lambda$ and $\partial^2 \mathbf{D}_o(\lambda^\varepsilon)/\partial\lambda_i^2$ respectively.

3. Insert equation (9) into equations (3) through (8).
4. Evaluate the derivatives of the displacement, quantities $L_i\delta_{ib}\frac{\partial \mathbf{D}_o(\lambda^\varepsilon)}{\partial \lambda_i}$, $L_i\delta_{ib}\frac{\partial \mathbf{D}_1^E(\lambda^\varepsilon)}{\partial \lambda_i}$, and $\frac{L_i^2\delta_{ib}^2}{2}\frac{\partial^2 \mathbf{D}_o(\lambda^\varepsilon)}{\partial \lambda_i^2}$, in the Cartesian basis (see equations (41)–(43) in [85]).
5. Write the equilibrium forces and moments in virtual power form

$$\sum_{\nu^i \in \mathbb{Z}^2}\sum_{b \in B_R}\left(T^b\dot{V} + N^b\dot{U}\right) = 0 \quad (10)$$

$$\sum_{\nu^i \in \mathbb{Z}^2}\sum_{b \in B_R}\left(\boldsymbol{M}_O^b.\mathbf{w}_O^b + \boldsymbol{M}_E^b.\mathbf{w}_E^b + \frac{l^b}{2}\left(\mathbf{e}^b \wedge \mathbf{F}_E^b\right).\mathbf{w}_C^b - \frac{l^b}{2}\left(\mathbf{e}^b \wedge \mathbf{F}_O^b\right).\mathbf{w}_C^b\right) = 0 \quad (11)$$

The moments are self-equilibrated; therefore the moment equilibrium is automatically satisfied.

B_R refers to the set of beams with in the reference unit cell, $\mathbf{w}$ the virtual rotation velocity and $\mathbf{F}^b = N^b\mathbf{e}^b + T^b\mathbf{e}^{b\perp}$ the force exerted on the beamb.

6. Write the virtual power of internal forces over an elementary cell (on the boundary nodes, since the contribution of the internal nodes mutually cancel):

$$P_e = \sum_b\left(T_E\left(\dot{V}_E - \dot{V}_O\right) + N_E\left(\dot{U}_E - \dot{U}_O\right)\right) \quad (12)$$

with $\dot{V}_i$ and $\dot{U}_i$ therein the two components of the virtual velocity field.

7. Development of the expressions of the relative longitudinal and transverse velocities $\left(\dot{V}_E - \dot{V}_O\right)$ and $\left(\dot{U}_E - \dot{U}_O\right)$ using a Taylor series expansion (see equation (53) in [85]).
8. Write the continuous formulation of the virtual power by passing to the limit in equation (12). One can find after development:

$$\lim_{\varepsilon\to 0} P = \lim_{\varepsilon\to 0} \varepsilon^2 \sum_{c\in\mathbb{Z}} P_e$$
$$= \int_{\Omega} P_e d\lambda = \int_{\Omega} \left[\frac{1}{g} \sum_{b} \left[\begin{array}{l} \left(\left(T_E^1 L_i \delta_{ib} \frac{\partial \dot{V}_o(\lambda^\varepsilon)}{\partial \lambda_i} \right) + \left(N_E^1 L_i \delta_{ib} \frac{\partial \dot{U}_o(\lambda^\varepsilon)}{\partial \lambda_i} \right) \right) \\ + \varepsilon \left(\begin{array}{l} \left(T_E^1 \frac{L_i^2 \delta_{ib}^2}{2} \frac{\partial^2 \dot{V}_o(\lambda^\varepsilon)}{\partial \lambda_i^2} \right) + \left(T_E^2 L_i \delta_{ib} \frac{\partial \dot{V}_o(\lambda^\varepsilon)}{\partial \lambda_i} \right) \\ + \left(N_E^1 \frac{L_i^2 \delta_{ib}^2}{2} \frac{\partial^2 \dot{U}_o(\lambda^\varepsilon)}{\partial \lambda_i^2} \right) + \left(N_E^2 L_i \delta_{ib} \frac{\partial \dot{U}_o(\lambda^\varepsilon)}{\partial \lambda_i} \right) \end{array} \right) \\ + \varepsilon^2 \left(\left(T_E^2 \frac{L_i^2 \delta_{ib}^2}{2} \frac{\partial^2 \dot{V}_o(\lambda^\varepsilon)}{\partial \lambda_i^2} \right) + \left(N_E^2 \frac{L_i^2 \delta_{ib}^2}{2} \frac{\partial^2 \dot{U}_o(\lambda^\varepsilon)}{\partial \lambda_i^2} \right) \right) \end{array} \right] \right] dV \tag{13}$$

with $N_E = \left(\varepsilon N_E^1 + \varepsilon^2 N_E^2\right)$, $T_E = \left(\varepsilon T_E^1 + \varepsilon^2 T_E^2\right)$ and g is the Jacobean of the transformation from Cartesian to curvilinear coordinates. Factor δ_i is the shift factor equal to ± 1 for nodes belonging to a neighboring cell, and nil for nodes located inside the considered cell.

Previous expression involves three integrals of increasing powers with respect to the scale parameter ε, namely the zero-order term (the factor ε^2 is absorbed into the continuation of the discrete sum towards Riemann integral), the first order representing coupling terms, and the second-order associated to the hyperstress tensor contribution. Previous expression is next written in Cartesian coordinates (see Appendix A).

9. Equivalence with a second-order grade continuum [10,84] in order to express the stress and hyperstress tensors

$$P^i = \int_{\Omega} ((\boldsymbol{\sigma} - \boldsymbol{S} \cdot \nabla) \cdot \nabla) \cdot \dot{\mathbf{D}}\, dV = \int_{\Omega} \left(\boldsymbol{F}^q \cdot \left(\frac{\partial \dot{\mathbf{D}}}{\partial x_q} \right) - \boldsymbol{H}^{pq} \cdot \left(\frac{\partial^2 \dot{\mathbf{D}}}{\partial x_p \partial x_q} \right) \right) dV \tag{14}$$

Second-order tensor $\dot{\mathbf{D}}$ therein is the virtual rate of deformation, $\boldsymbol{\sigma}$ is the Cauchy stress and $\mathbf{S}$ is the third-order hyperstress tensor with index symmetry $S_{ijk} = S_{ikj}$. The 3D spatial gradient operator has been denoted with the nabla operator ∇.

10. Calculation of the stress and hyperstress tensors, resulting in the following relations:

$$\boldsymbol{\sigma} = \left(\sigma_{iq} e_i\right) \otimes e_q = F^q \otimes e_q \tag{15}$$

$$\boldsymbol{S} = \left(S_{kqp} e_k\right) \otimes e_q \otimes e_p = H^{pq} \otimes e_q \otimes e_p \tag{16}$$

Such as $q \in \{1, 2\}$,

$$\mathbf{F}^1 = \left[\left(\frac{\mathbf{T}_E^1 + \mathbf{N}_E^1}{g} \right) + \varepsilon \left(\frac{\mathbf{T}_E^2 + \mathbf{N}_E^2}{g} \right) \right] (L_1 \delta_{1b} \cos\theta_1 + L_2 \delta_{2b} \cos\theta_2) \tag{17}$$

$$\mathbf{F}^2 = \left[\left(\frac{\mathbf{T}_E^1 + \mathbf{N}_E^1}{g} \right) + \varepsilon \left(\frac{\mathbf{T}_E^2 + \mathbf{N}_E^2}{g} \right) \right] (L_1 \delta_{1b} \sin\theta_1 + L_2 \delta_{2b} \sin\theta_2) \tag{18}$$

with the pair of indices $(p, q) \in \{(1,1), (2,2), (1,2)\}$,

$$\mathbf{H}^{11} = \left[\varepsilon \left(\frac{\mathbf{T}_E^1 + \mathbf{N}_E^1}{g} \right) + \varepsilon^2 \left(\frac{\mathbf{T}_E^2 + \mathbf{N}_E^2}{g} \right) \right] \left(\frac{L_1^2 \delta_{1b}{}^2 \cos^2\theta_1}{2} + \frac{L_2^2 \delta_{2b}{}^2 \cos^2\theta_2}{2} \right) \tag{19}$$

$$\mathbf{H}^{22} = \left[\varepsilon \left(\frac{\mathbf{T}_E^1 + \mathbf{N}_E^1}{g} \right) + \varepsilon^2 \left(\frac{\mathbf{T}_E^2 + \mathbf{N}_E^2}{g} \right) \right] \left(\frac{L_1^2 \delta_{1b}{}^2 \sin^2\theta_1}{2} + \frac{L_2^2 \delta_{2b}{}^2 \sin^2\theta_2}{2} \right) \tag{20}$$

$$\mathbf{H}^{12} = \left[\varepsilon\left(\frac{\mathbf{T}_E^1 + \mathbf{N}_E^1}{g}\right) + \varepsilon^2\left(\frac{\mathbf{T}_E^2 + \mathbf{N}_E^2}{g}\right)\right]\left(L_1^2\,\delta_{1b}{}^2\cos\theta_1\sin\theta_1 + L_2^2\,\delta_{2b}{}^2\sin\theta_2\cos\theta_2\right) \tag{21}$$

with $g = L_1L_2(\cos\theta_1\sin\theta_2 - \sin\theta_1\cos\theta_2)$ in the above the determinant of the Jacobian matrix and $\mathbf{T}_E^1 = T_E^1\mathbf{e}^{b\perp}$, $\mathbf{T}_E^2 = T_E^2\mathbf{e}^{b\perp}$, $\mathbf{N}_E^1 = N_E^1\mathbf{e}^b$; $\mathbf{N}_E^2 = N_E^2\mathbf{e}^b$.

The resultants expand on two orders versus ε, adopting the following choices of the exponents $\alpha = \beta = 1$ in equations (1) and (2):

$$\begin{aligned} N_E &= \varepsilon N_E^1 + \varepsilon^2 N_E^2 = \tilde{k}_l^b\left(\varepsilon(U_{E1} - U_{O1}) + \varepsilon^2(U_{E2} - U_{O2})\right) \\ &= \varepsilon\left(k_l^b(U_{E1} - U_{O1})\right) + \varepsilon^2\left(k_l^b(U_{E2} - U_{O2}) + 2E_B(U_{E1} - U_{O1})\right) \end{aligned} \tag{22}$$

$$\begin{aligned} T_E &= \varepsilon T_E^1 + \varepsilon^2 T_E^2 = \tilde{k}_f^b\left(\varepsilon(V_{E1} - V_{O1}) + \varepsilon^2(V_{E2} - V_{O2})\right) \\ &= \varepsilon(k_f^b(V_{E1} - V_{O1})) + \varepsilon^2(k_f^b(V_{E2} - V_{O2}) + 4\eta^2 E_B(V_{E1} - V_{O1})) \end{aligned} \tag{23}$$

The different terms in equations (22) and (23) are defined as follows:

$$U_{O1} = \mathbf{D}_1^O.\ \mathbf{e}^b\ ,\ U_{E1} = \left(\mathbf{D}_1^E + L_i\delta_{ib}\frac{\partial\mathbf{D}_o(\lambda^\varepsilon)}{\partial\lambda_i}\right).\ \mathbf{e}^b$$

$$U_{O2} = \mathbf{D}_2^O.\ \mathbf{e}^b,\ U_{E2} = \left(\mathbf{D}_2^E + L_i\delta_{ib}\frac{\partial\mathbf{D}_1^E(\lambda^\varepsilon)}{\partial\lambda_i} + \frac{L_i^2\delta_{ib}^2}{2}\frac{\partial^2\mathbf{D}_o(\lambda^\varepsilon)}{\partial\lambda_i^2}\right).\ \mathbf{e}^b$$

$$V_{O1} = \mathbf{D}_1^O.\ \mathbf{e}^{b\perp},\ V_{E1} = \left(\mathbf{D}_1^E + L_i\delta_{ib}\frac{\partial\mathbf{D}_o(\lambda^\varepsilon)}{\partial\lambda_i}\right).\ \mathbf{e}^{b\perp}$$

$$V_{O2} = \mathbf{D}_2^O.\ \mathbf{e}^{b\perp},\ V_{E2} = \left(\mathbf{D}_2^E + L_i\delta_{ib}\frac{\partial\mathbf{D}_1^E(\lambda^\varepsilon)}{\partial\lambda_i} + \frac{L_i^2\delta_{ib}^2}{2}\frac{\partial^2\mathbf{D}_o(\lambda^\varepsilon)}{\partial\lambda_i^2}\right).\ \mathbf{e}^{b\perp}$$

Owing to the linearity of the problem, the local displacements can be expressed in terms of the macro-strain using the localization operators for the strain and strain gradient loading terms (applied to the unit cell), so that it formally holds the following relations at first and second orders of the small-scale parameter:

$$\begin{aligned} (\mathbf{U}_{E1} - \mathbf{U}_{O1}) &= H^{E,1}.\mathbf{E} + H^{K,1}.\mathbf{K} \\ (\mathbf{U}_{E2} - \mathbf{U}_{O2}) &= H^{E,2}.\mathbf{E} + H^{K,2}.\mathbf{K} \end{aligned} \tag{24}$$

with $H^{E,1}, H^{K,1}, H^{E,2}, H^{K,2}$ therein the localization operators (each function of the microscopic variable within the unit cell) for the displacement at the first and second orders of the small parameter ε. These localization operators are obtained by solving the localization problems successively at the two orders using the equilibrium of forces and moments for the unit cell. They allow expression of the homogenized constitutive law, when inserting equation (24) into equations (15) and (16) and using the following scalings of the beam rigidities:

$$\tilde{k}_l = k_l + E_B\left(\varepsilon^\beta + \varepsilon^\alpha\right) + \frac{E_B}{\eta}\varepsilon^{\alpha+\beta},\ \tilde{k}_f = k_f + 3\eta^2E_B\varepsilon^\beta + E_B\eta^2\varepsilon^\alpha + 3E_B\eta\varepsilon^{\alpha+\beta} \tag{25}$$

$$\boldsymbol{\sigma} = \frac{1}{g}\left[\begin{pmatrix}\tilde{k}_f^b\left((H^{E,1}.\mathbf{E} + H^{K,1}.\mathbf{K}).\mathbf{e}^{b\perp}\right)\mathbf{e}^{b\perp} \\ +\tilde{k}_l^b\left((H^{E,1}.\mathbf{E} + H^{K,1}.\mathbf{K}).\mathbf{e}^b\right)\mathbf{e}^b\end{pmatrix} + \varepsilon\begin{pmatrix}\tilde{k}_f^b\left((H^{E,2}.\mathbf{E} + H^{K,2}.\mathbf{K}).\mathbf{e}^{b\perp}\right)\mathbf{e}^{b\perp} \\ +\tilde{k}_l^b\left((H^{E,2}.\mathbf{E} + H^{K,2}.\mathbf{K}).\mathbf{e}^b\right)\mathbf{e}^b\end{pmatrix}\right] \otimes \mathbf{B} = \boldsymbol{\sigma}_c + \boldsymbol{\sigma}_s \tag{26}$$

$$\mathbf{B} = \left(L_1\delta_1 c_{\theta_1} + L_2\delta_2 c_{\theta_2}\right) \otimes \mathbf{e}_1 + \left(L_1\delta_1 s_{\theta_1} + L_2\delta_2 s_{\theta_2}\right) \otimes \mathbf{e}_2$$

where $c_\theta, s_\theta, c_\theta^2$ and s_θ^2 stand for $\cos\theta$, $\sin\theta$, $\cos^2\theta$ and $\sin^2\theta$ and introducing therein the classical and surface Cauchy stress tensors $\boldsymbol{\sigma}_c, \boldsymbol{\sigma}_s$, expressed by

$$\boldsymbol{\sigma}_c = \frac{1}{g}\left[\begin{pmatrix} k_f^b\left((H^{E,1}.\mathbf{E}+H^{K,1}.\mathbf{K}).\mathbf{e}^{b\perp}\right)\mathbf{e}^{b\perp} \\ +k_l^b\left((H^{E,1}.\mathbf{E}+H^{K,1}.\mathbf{K}).\mathbf{e}^{b}\right)\mathbf{e}^{b} \end{pmatrix} + \varepsilon\begin{pmatrix} k_f^b\left((H^{E,2}.\mathbf{E}+H^{K,2}.\mathbf{K}).\mathbf{e}^{b\perp}\right)\mathbf{e}^{b\perp} \\ +k_l^b\left((H^{E,2}.\mathbf{E}+H^{K,2}.\mathbf{K}).\mathbf{e}^{b}\right)\mathbf{e}^{b} \end{pmatrix}\right]\otimes\mathbf{B}, \tag{27}$$

$$\boldsymbol{\sigma}_s = \frac{E_B}{g}\left[\begin{array}{l} \begin{pmatrix} (3\eta^2\varepsilon^\beta+\eta^2\varepsilon^\alpha+3\eta\varepsilon^{\alpha+\beta})\left((H^{E,1}.\mathbf{E}+H^{K,1}.\mathbf{K}).\mathbf{e}^{b\perp}\right)\mathbf{e}^{b\perp} \\ +\left((\varepsilon^\beta+\varepsilon^\alpha)+\frac{1}{\eta}\varepsilon^{\alpha+\beta}\right)\left((H^{E,1}.\mathbf{E}+H^{K,1}.\mathbf{K}).\mathbf{e}^{b}\right)\mathbf{e}^{b} \end{pmatrix} + \\ \varepsilon\begin{pmatrix} (3\eta^2\varepsilon^\beta+\eta^2\varepsilon^\alpha+3\eta\varepsilon^{\alpha+\beta})\left((H^{E,2}.\mathbf{E}+H^{K,2}.\mathbf{K}).\mathbf{e}^{b\perp}\right)\mathbf{e}^{b\perp} \\ +\left((\varepsilon^\beta+\varepsilon^\alpha)+\frac{1}{\eta}\varepsilon^{\alpha+\beta}\right)\left((H^{E,2}.\mathbf{E}+H^{K,2}.\mathbf{K}).\mathbf{e}^{b}\right)\mathbf{e}^{b} \end{pmatrix} \end{array}\right]\otimes\mathbf{B}$$

It holds similarly for the hyperstress the decomposition into a classical contribution (in the absence of surface effects) and an additional term accounting for surface effects, equation (26):

$$\begin{aligned} \mathbf{S} &= \frac{1}{g}\left(\varepsilon\begin{pmatrix} \tilde{k}_f^b\left((H^{E,1}.\mathbf{E}+H^{K,1}.\mathbf{K}).\mathbf{e}^{b\perp}\right)\mathbf{e}^{b\perp} \\ +\tilde{k}_l^b\left((H^{E,1}.\mathbf{E}+H^{K,1}.\mathbf{K}).\mathbf{e}^{b}\right)\mathbf{e}^{b} \end{pmatrix} + \varepsilon^2\begin{pmatrix} \tilde{k}_f^b\left((H^{E,2}.\mathbf{E}+H^{K,2}.\mathbf{K}).\mathbf{e}^{b\perp}\right)\mathbf{e}^{b\perp} \\ +\tilde{k}_l^b\left((H^{E,2}.\mathbf{E}+H^{K,2}.\mathbf{K}).\mathbf{e}^{b}\right)\mathbf{e}^{b} \end{pmatrix}\right)\otimes\mathbf{A}, \\ &= \mathbf{S}_c+\mathbf{S}_s \\ \mathbf{A} &= \left(\frac{L_1^2\delta_1^2c_{\theta_1}^2}{2}+\frac{L_2^2\delta_2^2c_{\theta_2}^2}{2}\right)\mathbf{e}_1\otimes\mathbf{e}_1+\left(\frac{L_1^2\delta_1^2s_{\theta_1}^2}{2}+\frac{L_2^2\delta_2^2s_{\theta_2}^2}{2}\right)\mathbf{e}_2\otimes\mathbf{e}_2+ \\ &+\left(L_1^2\delta_1^2c_{\theta_1}s_{\theta_1}+L_2^2\delta_2^2s_{\theta_2}c_{\theta_2}\right)(\mathbf{e}_1\otimes\mathbf{e}_2+\ \otimes\mathbf{e}_2\otimes\mathbf{e}_1) \end{aligned} \tag{28}$$

introducing therein the classical and surface hyperstress tensors $\mathbf{S}_c, \mathbf{S}_s$ expressed as

$$\mathbf{S}_c = \frac{1}{g}\left(\varepsilon\begin{pmatrix} k_f^b\left((H^{E,1}.\mathbf{E}+H^{K,1}.\mathbf{K}).\mathbf{e}^{b\perp}\right)\mathbf{e}^{b\perp} \\ +k_l^b\left((H^{E,1}.\mathbf{E}+H^{K,1}.\mathbf{K}).\mathbf{e}^{b}\right)\mathbf{e}^{b} \end{pmatrix} + \varepsilon^2\begin{pmatrix} k_f^b\left((H^{E,2}.\mathbf{E}+H^{K,2}.\mathbf{K}).\mathbf{e}^{b\perp}\right)\mathbf{e}^{b\perp} \\ +k_l^b\left((H^{E,2}.\mathbf{E}+H^{K,2}.\mathbf{K}).\mathbf{e}^{b}\right)\mathbf{e}^{b} \end{pmatrix}\right)\otimes\mathbf{A},$$

$$\mathbf{S}_s = \frac{E_B}{g}\left(\begin{array}{l} \varepsilon\begin{pmatrix} (3\eta^2\varepsilon^\beta+\eta^2\varepsilon^\alpha+3\eta\varepsilon^{\alpha+\beta})\left((H^{E,1}.\mathbf{E}+H^{K,1}.\mathbf{K}).\mathbf{e}^{b\perp}\right)\mathbf{e}^{b\perp} \\ +\left((\varepsilon^\beta+\varepsilon^\alpha)+\frac{1}{\eta}\varepsilon^{\alpha+\beta}\right)\left((H^{E,1}.\mathbf{E}+H^{K,1}.\mathbf{K}).\mathbf{e}^{b}\right)\mathbf{e}^{b} \end{pmatrix} \\ +\varepsilon^2\begin{pmatrix} (3\eta^2\varepsilon^\beta+\eta^2\varepsilon^\alpha+3\eta\varepsilon^{\alpha+\beta})\left((H^{E,2}.\mathbf{E}+H^{K,2}.\mathbf{K}).\mathbf{e}^{b\perp}\right)\mathbf{e}^{b\perp} \\ +\left((\varepsilon^\beta+\varepsilon^\alpha)+\frac{1}{\eta}\varepsilon^{\alpha+\beta}\right)\left((H^{E,2}.\mathbf{E}+H^{K,2}.\mathbf{K}).\mathbf{e}^{b}\right)\mathbf{e}^{b} \end{pmatrix} \end{array}\right)\otimes\mathbf{A} \tag{29}$$

Note that the classical contribution in both the classical stress tensor and the hyperstress tensor appears at two orders versus the scale parameter ε. Surface effects appear in the (surface) stress and hyperstress tensors as higher-order contributions versus the scale parameter ε in comparison to their classical contribution (in the absence of surface effects). Surface effects may dominate over classical contributions when at least one of the exponents α, β is negative; in such a situation, that the surface effects present in the strain gradient terms outweigh the classical Cauchy-type response of the material.

When both exponents α, β vanish, there is an additional surface contribution to the first-order beam rigidities. For the specific case $\alpha = 1 = \beta$, equations (1) and (2) lead to the modified beam rigidities

$$\tilde{k}_l = k_l + 2E_B\varepsilon + O(\varepsilon^2), \tilde{k}_f = k_f + 4\eta^2E_B\varepsilon + O(\varepsilon^2) \tag{30}$$

Inserting these expressions for the rigidities into equations (26) through (29) shows that surface effects appear at order ε in the (surface) Cauchy stress, whereas they are present at the next order ε^2 in the surface hyperstress tensor, which are written explicitly as follows:

$$\boldsymbol{\sigma}_s = \frac{\mathrm{E}_B}{g}\left[\begin{array}{l}\left(\begin{array}{l}(4\eta^2\varepsilon+3\eta\varepsilon^2)\left((H^{E,1}.\mathbf{E}+H^{K,1}.\mathbf{K}).\mathbf{e}^{b^\perp}\right)\mathbf{e}^{b^\perp}\\ +\left(2\varepsilon+\frac{1}{\eta}\varepsilon^2\right)\left((H^{E,1}.\mathbf{E}+H^{K,1}.\mathbf{K}).\mathbf{e}^{b}\right)\mathbf{e}^{b}\end{array}\right)+\\ \varepsilon\left(\begin{array}{l}(4\eta^2\varepsilon+3\eta\varepsilon^2)\left((H^{E,2}.\mathbf{E}+H^{K,2}.\mathbf{K}).\mathbf{e}^{b^\perp}\right)\mathbf{e}^{b^\perp}\\ +\left(2\varepsilon+\frac{1}{\eta}\varepsilon^2\right)\left((H^{E,2}.\mathbf{E}+H^{K,2}.\mathbf{K}).\mathbf{e}^{b}\right)\mathbf{e}^{b}\end{array}\right)\end{array}\right]\otimes\mathbf{B}, \tag{31}$$

$$\mathbf{S}_s = \frac{\mathrm{E}_B}{g}\left(\begin{array}{l}\varepsilon^2\left(\begin{array}{l}(4\eta^2+3\eta\varepsilon)\left((H^{E,1}.\mathbf{E}+H^{K,1}.\mathbf{K}).\mathbf{e}^{b^\perp}\right)\mathbf{e}^{b^\perp}\\ +\left(2+\frac{1}{\eta}\varepsilon\right)\left((H^{E,1}.\mathbf{E}+H^{K,1}.\mathbf{K}).\mathbf{e}^{b}\right)\mathbf{e}^{b}\end{array}\right)+\\ \varepsilon^3\left(\begin{array}{l}(4\eta^2+3\eta\varepsilon)\left((H^{E,2}.\mathbf{E}+H^{K,2}.\mathbf{K}).\mathbf{e}^{b^\perp}\right)\mathbf{e}^{b^\perp}\\ +\left(2+\frac{1}{\eta}\varepsilon\right)\left((H^{E,2}.\mathbf{E}+H^{K,2}.\mathbf{K}).\mathbf{e}^{b}\right)\mathbf{e}^{b}\end{array}\right)\end{array}\right)\otimes\mathbf{A} \tag{32}$$

The obtained expressions of the surface stress and hyperstress tensors show that the slenderness ratio of the beam play a determinant role since it determines the relative importance of surface effects on the effective mechanical properties.

In the next section we provide an example of a non-centrosymmetric beam-like network in order to show the importance of surface effects on the effective mechanical properties of the homogenized second gradient continuum.

3. Non-centrosymmetric square unit-cell network material architectures

The methodology presented in Section 2.1 is general, provided a repetitive unit cell can been identified. In the current section, we apply the previously elaborated methodology to the 2D square-shaped unit-cell structure with two internal beams that do not intersect in their center pictured in Figure 3, so that it is not centrosymmetric and coupling effects between first and second gradient contributions are expected. The unit cell is composed of a total of eight beam elements, as shown in Figure 3.

The mechanical parameters selected in this example originate from experimental data obtained with tensile tests of single crystal ZnO nanowires having a [0001] oriented wurtzite structure from Agrawal et al. [85]. The geometrical and mechanical parameters of the unit-cell structure are conveniently summarized in Table 1.

The vector including all beam lengths is elaborated as

$$L_b = \left[\frac{L}{2}, \frac{L}{2}, \frac{L}{2}, \frac{L}{2}, \frac{L}{2\sqrt{2}}, \frac{3\sqrt{2}L}{4}, \frac{L}{2\sqrt{2}}, \frac{L}{2\sqrt{2}}\right],$$

and the periodicity vectors used to generate the periodic planar network are $Y_1 = \begin{bmatrix}1\\0\end{bmatrix}$, $Y_2 = \begin{bmatrix}0\\1\end{bmatrix}$ with respective lengths $L_1 = L_2 = L$. We adopt the angular value $\theta = 45^\circ$. The connectivity table of this lattice is provided in Table 2. All beams have here the same mechanical properties.

The constitutive law for an anisotropic second gradient continuum is written as follows:

$$\sigma_{ij} = C_{ijpq}\,\epsilon_{pq} + M_{pqrij}\,K_{pqr}$$
$$S_{ijk} = M_{ijkpq}\,\epsilon_{pq} + A_{ijkpqr}\,K_{pqr}$$

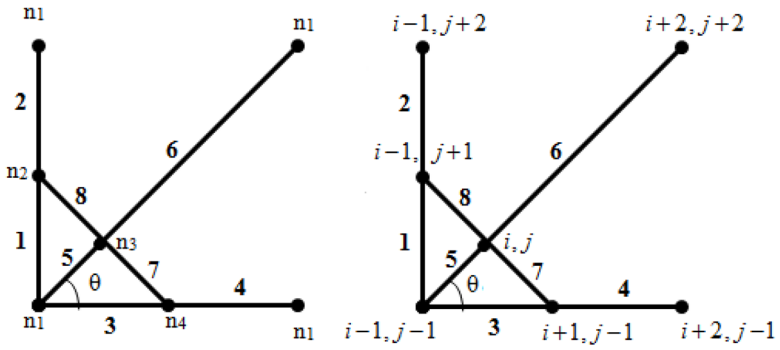

Figure 3. Unit cell of the square structure with internal crossed beams.

Table 1. Geometrical and mechanical parameters of the square lattice.

Type	Geometric parameters of the beam	Mechanical properties
Square	$L = 10\,\text{mm}$, $\beta = 45^{\circ}$, $t = 1\,\text{mm(width)}$	$E_B = 56.2\text{GPa}$, $\nu = 0.3$

Table 2. Connectivity table of the square lattice.

Beam	1	2	3	4	5	6	7	8
O(b)	1	2	1	4	1	3	4	3
E(b)	2	1	4	1	3	1	3	2
δ^1	0	0	0	1	0	1	0	0
δ^2	0	1	0	0	0	1	0	0

introducing therein $\sigma_{ij}, S_{ijk}, \epsilon_{pq}$, and K_{pqr} the stress, hyperstress, deformation, and gradient of deformation tensors, respectively. The tensors $C_{ijpq}, A_{ijkpqr}, M_{pqrij}$ are the first- and second-order elasticity tensors and the coupling tensor, respectively.

One obtains for this example exhibiting a non-centrosymmetric microstructure the following homogenized tensors:

$$[C] = \begin{bmatrix} 7860 & 2010 & 1830 & 1850 \\ 2010 & 7860 & 1850 & 1830 \\ 1830 & 1850 & 2430 & 2040 \\ 1850 & 1830 & 2040 & 2430 \end{bmatrix}; \quad [M] = \begin{bmatrix} 39300 & 10000 & 9140 & 9240 & 0 & 0 \\ 10000 & 39300 & 9240 & 9140 & 0 & 0 \\ 9140 & 9240 & 10200 & 12100 & 0 & 0 \\ 9240 & 9140 & 12100 & 10200 & 0 & 0 \end{bmatrix}$$

$$[A] = \begin{bmatrix} 2.44\,10^5 & 94400 & 97200 & 1.05\,10^5 & 0 & 0 \\ 94400 & 2.44\,10^5 & 1.05\,10^5 & 94400 & 0 & 0 \\ 97200 & 1.05\,10^5 & 1.05\,10^5 & 2.44\,10^5 & 0 & 0 \\ 1.05\,10^5 & 94400 & 2.44\,10^5 & 1.05\,10^5 & 0 & 0 \\ 0 & 0 & 0 & 0 & 0 & 0 \\ 0 & 0 & 0 & 0 & 0 & 0 \end{bmatrix}$$

The dimensions of the coefficients of these effective rigidity tensors are as follows: [C] n Pa, [M] in Pa m, and [A] in N.

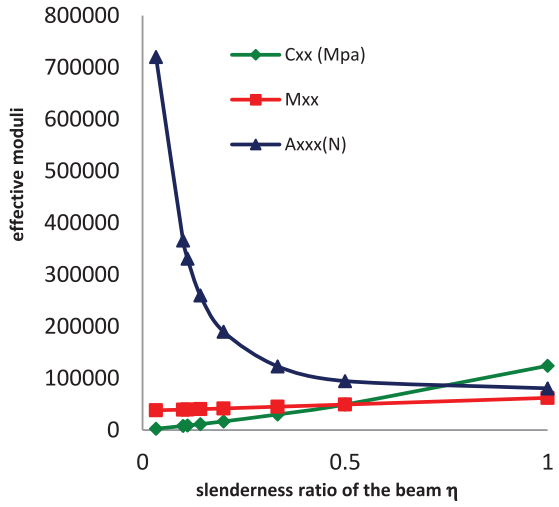

Figure 4. Evolution of the effective moduli versus the slenderness ratio of the beam.

If we compare these results with those of the case without surface effects, one notes that the tensors of classical and coupling moduli, **C** and **M** do not change while the components of the second gradient tensor **A** are increased by about 23% when surface effects are accounted for.

The effective moduli C_{xx}, M_{xx}, and A_{xxx} are represented versus parameters η and E_B in Figure 4; the second-order tensile modulus A_{xxx} is maximum for pure tensile lattices (η tends to 0), and it decreases towards a minimum when η tends to 1 contrary to C_{xx} and M_{xx}. In order to verify the asymptotic expansion method, an analytical method based on an evaluation at micro-level of the strain energy density is presented in the Appendix B. Both identification procedures lead to the construction of the same second gradient linear continuum. Indeed its effective mechanical properties can be obtained by means of either. For more complex structures, the asymptotic homogenization is quite efficient (in comparison, analytical methods become quite complicated and inapplicable). Let us note that the influence of surface elastic moduli on the effective material properties of nanosized network materials, such as nanofoams, is similar to the case of nanoporous solids [70,71].

4. Conclusion

Surface effects of network materials caused by a thin coating of the structural beam elements have been introduced in the present work. A discrete asymptotic expansion method has been used to derive the expressions of Cauchy stress and hyperstress tensors for the adopted effective strain gradient continuum. Surface effects are accounted for by two small parameters, the ratio of the surface modulus of the coating to the bulk modulus of the beam material, and the ratio of the thickness coating to the beam length. These two parameters are made dependent upon the scaling parameter (ratio of the representative unit cell size to a macroscopic characteristic length) according to two different scaling laws, thereby introducing two scaling exponent. Thereby, surface effects appear in second gradient contributions to the constitutive law (in the hyperstress tensor) for non-negative values of the scaling exponents; this corresponds to the typical situation, described in the pioneering work of Mindlin [16] wherein the strain gradient continuum is motivated by its ability to incorporate surface effects through the strain gradient terms. In the present work, the additional surface properties of the effective constitutive law emerge in the asymptotic expansion of the effective stress and hyperstress tensors versus the small-scale parameters and the additional small parameters related to surface effects. The range of possible values of the scaling exponents allows envisaging different models in which the importance of surface effects is dictated by specific choice of the scaling relations between the introduced small parameters. We show especially that surface effects may become dominant for specific choices of the scaling laws of the introduced small parameters. The example of a non-centrosymmetric repetitive network for which couplings between first and second gradient effects appear has been chosen to illustrate the proposed general methodology. The proposed

model of surface effects in network materials shall prove useful for the prediction of the importance of surface contributions of network materials and architectured media, especially at the very small scales (nanometric level); its predictive capacity further allows conceiving and optimizing microstructures based on the elaboration of specific requirements at the continuum level.

Declaration of conflicting interests

The author(s) declared no potential conflicts of interest with respect to the research, authorship, and/or publication of this article.

Funding

The author(s) disclosed receipt of the following financial support for the research, authorship, and/or publication of this article: VAE gratefully acknowledges the financial support from LEM3, University of Lorraine, during his visit in Nancy in 2018.

References

[1] Sanchez-Hubert, J, and Sanchez-Palencia, E. *Introduction aux méthodes asymptotiques et à l'homogénéisation: application à la mécanique des milieux continus*. Paris: Masson, 1992.
[2] Bornet, M, Bretheau, T, and Gilormini, P. *Homogénéisation en mécanique des matériaux 1*. Hermes Sciences, 2001.
[3] El Jarroudi, M, and Brillard, A. Asymptotic behaviour of a cylindrical elastic structure periodically reinforced along identical fibres. *IMA J Appl Math* 2001; 66: 567–590.
[4] Bellieud, M, and Bouchitté, G. Homogenization of a soft elastic material reinforced by fibers. *Asymptotic Anal* 2002; 32: 153–183.
[5] Sili, A. Homogenization of an elastic medium reinforced by anisotropic fibers. *Asymptotic Anal* 2005; 42: 133–171.
[6] Dos Reis, F, and Ganghoffer, JF. Discrete homogenization of architectured materials: Implementation of the method in a simulation tool for the systematic prediction of their effective elastic properties. *Tech Mech* 2010; 30: 85-109.
[7] Dos Reis, F, and Ganghoffer, JF. Construction of micropolar continua from the asymptotic homogenization of beam lattices. *Comput Struct* 2012; 112–113: 354–363.
[8] Askes, H, and Aifantis, EC. Gradient elasticity in statics and dynamics: an overview of formulations, length scale identification procedures, finite element implementations and new results. *Int J Solids Struct* 2011; 48: 1962–1990.
[9] Trinh, DK, Jänicke, R, Auffray, N, et al. Evaluation of generalized continuum substitution models for heterogeneous materials. *Int J Multiscale Comput Eng* 2011; 10: 527-549.
[10] Forest, S. *Milieux continus généralisés et matériaux hétérogènes*. Paris: Presses de l'École des Mines, 2006.
[11] Auffray, N, dell'Isola, F, Eremeyev, V, et al. Analytical continuum mechanics a la Hamilton-Piola: least action principle for second gradient continua and capillary fluids. *Math Mech Solids* 2015; 20: 375-417.
[12] Dell'Isola, F, Giorgio, I, and Andreaus, U. Elastic pantographic 2D lattices: a numerical analysis on static response and wave propagation. *Proc Est Acad Sci* 2014; 64: 219-225.
[13] Cosserat, E, and Cosserat, F. *Théorie des corps déformables*. Paris : Herman et Fils, 1909.
[14] Toupin, R. Elastic materials with couple stresses. *Arch Ration Mech Anal* 1962; 11: 385–413.
[15] Mindlin, RD. Microstructure in linear elasticity. *Arch Ration Mech Anal* 1964; 16: 51–78.
[16] Mindlin, RD. Second gradient of strain and surface-tension in linear elasticity. *Int J Solids Struct* 1965; 1: 417–438.
[17] Germain, P. The method of virtual power in continuum mechanics. Part 2. Microstructure. *SIAM J Appl Math* 1973; 25: 556–575.
[18] Sedov, LI. Mathematical methods for constructing new models of continuous media. *Russ Math Surv* 1965; 20(5): 123.
[19] Cosserat, E, and Cosserat, F. Sur la théorie de l'élasticité. *Ann Fac Sci Toulouse Math* 1896 ; 10 : 1–116.
[20] Eringen, AC, and Suhubi, ES. Nonlinear theory of simple micro-elastic solids. *Int J Eng Sci* 1964; 2: 189–203.
[21] Mindlin, RD, and Eshel, NN. On first strain gradient theories in linear elasticity. *Int J Solids Struct* 1968; 4: 109–124.
[22] Chen, Y, Lee, JD, and Eskandarian, A. Atomistic viewpoint of the applicability of microcontinuum theories. *Int J Solids Struct* 2004; 41: 2085–2097.
[23] Edelen, DGB. Protoelastic bodies with large deformation. *Arch Ration Mech Anal* 1969; 34: 283–300.
[24] Eringen, AC. *Microcontinuum field theories. I. Foundations and solids*. New York: Springer-Verlag, 1999.
[25] Eringen, AC. A unified theory of thermomechanical materials. *Int J Eng Sci* 1966; 4: 179–202.
[26] Hadjesfandiari, AR, and Dargush, GF. Couple stress theory for solids. *Int J Solids Struct* 2011; 48: 2496–2510.
[27] Lam, DCC, Yang, F, Chong, ACM, et al. Experiments and theory in strain gradient elasticity. *J Mech Phys Solids* 2003; 51: 1477–1508.
[28] Mindlin, RD, and Tiersten, HF. Effects of couple stresses in linear elasticity. *Arch Ration Mech Anal* 1962; 11: 415–448.
[29] Polyzos, D, and Fotiadis, DI. Derivation of Mindlin's first and second-strain gradient elastic theory via simple lattice and continuum models. *Int J Solids Struct* 2012; 49: 470–480.

[30] Yang, F, Chong, ACM, Lam, DCC, et al. Couple stress based strain gradient theory for elasticity. *Int J Solids Struct* 2002; 39: 2731–2743.
[31] Forest, S. Mechanics of generalized continua: construction by homogenization. *J Phys IV* 1998; 8: 39–48.
[32] Forest, S. Homogenization methods and the mechanics of generalized continua. Part 2. *Theor Appl Mech* 2002; 28–29: 113–143.
[33] Kouznetsova, V, Geers, MGD, and Brekelmans, WAM. Multi-scale constitutive modelling of heterogeneous materials with a gradient–enhanced computational homogenization scheme. *Int J Numer Methods Eng* 2002; 54: 1235–1260.
[34] Desrues, J, and Viggiani, G. Strain localization in sand: an overview of the experimental results obtained in grenoble using stereophotogrammetry. *Int J Numer Anal Methods Geomech* 2004; 28: 279–321.
[35] Pideri, C, and Seppecher, P. A second gradient material resulting from the homogenization of a heterogeneous linear elastic medium. *Cont Mech Therm* 1997; 9: 241–257.
[36] Camar-Eddine, M, and Seppecher, P. Determination of the closure of the set of elasticity functionals. *Arch Ration Mech Anal* 2003; 170: 211–245.
[37] El Jarroudi, M. Homogenization of a nonlinear elastic fibre-reinforced composite: a second gradient nonlinear elastic material. *J Math Anal Appl* 2013; 403: 487–505.
[38] Chambon, R, Caillerie, D, and El Hassan, N. Étude de la localisation unidimensionnelle à l'aide d'un modèle de second gradient. *C R Acad Sci* 1996; 323: 231–238.
[39] Chambon, R, Caillerie, D, and El Hassan, N. One-dimensional localization studied with a second grade model. *Eur J Mech A Solids* 1998; 17: 637–656.
[40] Chambon, R, Caillerie, D, and Matsuchima, T. Plastic continuum with microstructure, local second gradient theories for geomaterials: localization studies. *Int J Solids Struct* 2001; 38: 8503–8527.
[41] Cuenot, S, Frétigny, C, Demoustier-Champagne, S, et al. Surface tension effect on the mechanical properties of nanomaterials measured by atomic force microscopy. *Phys Rev B* 2004; 69: 165410.
[42] Jing, GY, Duan, HL, Sun, XM, et al. Surface effects on elastic properties of silver nanowires: Contact atomic-force microscopy. *Phys Rev B* 2006; 73: 235409.
[43] Chen, C, Shi, Y, Zhang, Y, et al. Size dependence of Young's modulus in ZnO nanowires. *Phys Rev Lett* 2006; 96: 075505.
[44] He, J, and Lilley, CM. Surface effect on the elastic behavior of static bending nanowires. *Nano Lett* 2008; 8: 1798–1802.
[45] Liu, X, Luo, J, and Zhu, J. Size effect on the crystal structure of silver nanowires. *Nano Lett* 2006; 6: 408–412.
[46] Laplace, PS. Sur l'action capillaire. Supplément à la théorie de l'action capillaire. In: *Traité de mécanique céleste*, Vol. 4, Supplement 1, Livre X. Paris: Gauthier–Villars et fils, 1805, pp.771–777.
[47] Laplace, PS. À la théorie de l'action capillaire. Supplément à la théorie de l'action capillaire. In: *Traité de mécanique céleste*, Vol. 4, Supplement 2, Livre X. Paris: Gauthier–Villars et fils, 1806, pp.909–945.
[48] Young, T. An essay on the cohesion of fluids. *Philos Trans R Soc Lond* 1805; 95: 65–87.
[49] Poisson, SD. *Nouvelle théorie de l'action capillaire*. Paris: Bachelier Père et Fils, 1831.
[50] Longley, WR, and Name, RGV. *The collected works of J. Willard Gibbs, PhD, LLD. Volume I. Thermodynamics*. New York: Longmans, 1928.
[51] De Gennes, PG, Brochard-Wyart, F, and Quéré, D. *Capillarity and wetting phenomena: drops, bubbles, pearls, waves*. New York: Springer, 2004.
[52] Rowlinson, JS, and Widom, B. *Molecular theory of capillarity*. New York: Dover, 2003.
[53] Gurtin, ME, and Murdoch, AI. Addenda to our paper A continuum theory of elastic material surfaces. *Arch Ration Mech Anal* 1975; 59: 389–390.
[54] Gurtin, ME, and Murdoch, AI. A continuum theory of elastic material surfaces. *Arch Ration Mech Anal* 1975; 57: 291–323.
[55] Wang, J, Duan, HL, Huang, ZP, et al. A scaling law for properties of nano-structured materials. *Proc R Soc Lond A* 2006; 462: 1355–1363.
[56] Steigmann, DJ, and Ogden, RW. Plane deformations of elastic solids with intrinsic boundary elasticity. *Proc R Soc Lond A* 1997; 453: 853–877.
[57] Steigmann, DJ, and Ogden, RW. Elastic surface–substrate interactions. *Proc R Soc Lond A* 1999; 455: 437–474.
[58] Javili, A, McBride, A, and Steinmann, P. Thermomechanics of solids with lower-dimensional energetics: on the importance of surface, interface, and curve structures at the nanoscale, a unifying review. *Appl Mech Rev* 2012 65: 010802.
[59] Javili, A, dell'Isola, F, and Steinmann, P. Geometrically nonlinear higher-gradient elasticity with energetic boundaries. *J Mech Phys Solids* 2013; 61: 2381–2401.
[60] Podio-Guidugli, P, and Caffarelli, GV. Surface interaction potentials in elasticity. *Arch Ration Mech Anal* 1990; 109: 345-385.
[61] Povstenko, Y. Mathematical modeling of phenomena caused by surface stresses in solids. *Surf Effects Solid Mech* 2013; 30: 135–153.

[62] Šilhavý, M. A direct approach to nonlinear shells with application to surface–substrate interactions. *Math Mech Complex Syst* 2013; 1: 211–232.
[63] Lurie, S, and Belov, P. Gradient effects in fracturemechanics for nano-structured materials. *Eng Fract Mech* 2014; 130: 3–11.
[64] Lurie, SA, and Kalamkarov, AL. General theory of continuous media with conserved dislocations. *Int J Solids Struct* 2007; 44: 7468–7485.
[65] Lurie, SA, and Belov, PA. Cohesion field: Barenblatt's hypothesis as formal corollary of theory of continuous media with conserved dislocations. *Int J Fract* 2008; 150: 181–194.
[66] Lurie, S, Volkov-Bogorodsky, D, Zubov, V, et al. Advanced theoretical and numerical multiscale modeling of cohesion/adhesion interactions in continuum mechanics and its applications for filled nanocomposites. *Comput Mater Sci* 2009; 45: 709–714.
[67] Rubin, M, and Benveniste, Y. A Cosserat shell model for interphases in elastic media. *J Mech Phys Solids* 2004; 52: 1023-1052.
[68] Duan, HL, and Karihaloo, BL. Thermo-elastic properties of heterogeneous materials with imperfect interfaces: generalized Levin's formula and Hill's connections. *J Mech Phys Solids* 2007; 55: 1036–1052.
[69] Duan, HL, Wang, J, Huang, ZP, et al. Size-dependent effective elastic constants of solids containing nanoinhomogeneities with interface stress. *J Mech Phys Solids* 2005; 53: 1574–1596.
[70] Duan, HL, Wang, J, Karihaloo, BL, et al. Nanoporous materials can be made stiffer than non-porous counterparts by surface modification. *Acta Mater* 2006; 54: 2983–2990.
[71] Duan, HL, Wang, J, and Karihaloo, BL. Theory of elasticity at the nanoscale. *Adv Appl Mech* 2009; 42: 1–68.
[72] Kushch, VI, Chernobai, VS, and Mishuris, GS. Longitudinal shear of a composite with elliptic nanofibers: local stresses and effective stiffness. *Int J Eng Sci* 2014; 84: 79–94.
[73] Kushch, VI, Sevostianov, I, and Chernobai, VS. Effective conductivity of composite with imperfect contact between elliptic fibers and matrix: Maxwell's homogenization scheme. *Int J Eng Sci* 2014; 83: 146–161.
[74] Wang, J, Huang, Z, Duan, H, et al. Surface stress effect in mechanics of nanostructured materials. *Acta Mech Solida Sin* 2011; 24: 52–82.
[75] Altenbach, H, and Eremeyev, VA. On the shell theory on the nanoscale with surface stresses. *Int J Eng Sci* 2011; 49: 1294-1301.
[76] Altenbach, H, Eremeyev, VA, and Morozov, NF. Surface viscoelasticity and effective properties of thin-walled structures at the nanoscale. *Int J Eng Sci* 2012; 59: 83–89.
[77] Altenbach, H, Eremeyev, VA, and Morozov, NF (2013). Mechanical properties of materials considering surface effects. In: Cocks, A, and Wang, J (eds.) *IUTAM symposium on surface effects in the mechanics of nanomaterials and heterostructures*. Dordrecht: Springer, 2013, pp.105–115.
[78] Eremeyev, VA, Altenbach, H, and Morozov, NF. The influence of surface tension on the effective stiffness of nanosized plates. *Doklady Phys* 2009; 54: 98–100.
[79] Heinonen, S, Huttunen-Saarivirta, E, Nikkanen, JP, et al. Antibacterial properties and chemical stability of superhydrophobic silver-containing surface produced by sol–gel route. *Colloids Surf A Physicochem Eng Aspects* 2014; 453: 149–161.
[80] Wang, ZQ, Zhao, YP, and Huang, ZP. The effects of surface tension on the elastic properties of nano structures. *Int J Eng Sci* 2010; 48: 140–150.
[81] Guo, JG, and Zhao, YP. The size-dependent elastic properties of nanofilms with surface effects. *J Appl Phys* 2005; 98: 074306.
[82] Eremeyev, V. On effective properties of materials at the nano- and microscales considering surface effects. *Acta Mech* 2015; 227: 29–42.
[83] Rahali, Y, Dos Reis, F, and Ganghoffer, JF. Multiscale homogenization schemes for the construction of second order grade anisotropic continuum media of architectured materials. *J Multiscale Comput Eng* 2017; 15: 35–78.
[84] Rahali, Y, Giorgio, I, Ganghoffer, JF, et al. Homogenization à la Piola produces second gradient continuum models for linear pantographic lattices. *Int J Eng Sci* 2015; 97: 148-172.
[85] Agrawal, R, Peng, B, Gdoutos, EE, et al. Elasticity size effects in ZnO nanowires: a combined experimental-computational approach. *Nano Lett* 2008; 8: 3668–3674.

Appendix A

Transition from curvilinear to Cartesian coordinates

After development of equation (13) in Cartesian coordinates, one obtains

$$\lim_{\varepsilon\to 0} P = \int_{\Omega} \left[\frac{1}{g} \sum_{b} \left[\begin{array}{l} \left(\begin{array}{l} T_E^1 \left(L_1 \delta_{1b} \left(c_{\theta_1} \frac{\partial \dot{V}_o}{\partial x} + s_{\theta_1} \frac{\partial \dot{V}_o}{\partial y} \right) + L_2 \delta_{2b} \left(c_{\theta_2} \frac{\partial \dot{V}_o}{\partial x} + s_{\theta_2} \frac{\partial \dot{V}_o}{\partial y} \right) \right) \\ + N_E^1 \left(L_1 \delta_{1b} \left(c_{\theta_1} \frac{\partial \dot{U}_o}{\partial x} + s_{\theta_1} \frac{\partial \dot{U}_o}{\partial y} \right) + L_2 \delta_{2b} \left(c_{\theta_2} \frac{\partial \dot{U}_o}{\partial x} + s_{\theta_2} \frac{\partial \dot{U}_o}{\partial y} \right) \right) \end{array} \right) \\ + \varepsilon \left(\begin{array}{l} T_E^1 \left(\begin{array}{l} \frac{L_1^2 \delta_{1b}^2}{2} \left(c_{\theta_1}^2 \frac{\partial^2 \dot{V}_o}{\partial x^2} + s_{\theta_1}^2 \frac{\partial^2 \dot{V}_o}{\partial y^2} + 2 s_{\theta_1} c_{\theta_1} \frac{\partial^2 \dot{V}_o}{\partial x \partial y} \right) \\ + \frac{L_2^2 \delta_{2b}^2}{2} \left(c_{\theta_2}^2 \frac{\partial^2 \dot{V}_o}{\partial x^2} + s_{\theta_2}^2 \frac{\partial^2 \dot{V}_o}{\partial y^2} + 2 s_{\theta_2} c_{\theta_2} \frac{\partial^2 \dot{V}_o}{\partial x \partial y} \right) \end{array} \right) \\ + T_E^2 \left(L_1 \delta_{1b} \left(c_{\theta_1} \frac{\partial \dot{V}_o}{\partial x} + s_{\theta_1} \frac{\partial \dot{V}_o}{\partial y} \right) + L_2 \delta_{2b} \left(c_{\theta_2} \frac{\partial \dot{V}_o}{\partial x} + s_{\theta_2} \frac{\partial \dot{V}_o}{\partial y} \right) \right) \\ + N_E^1 \left(\begin{array}{l} \frac{L_1^2 \delta_{1b}^2}{2} \left(c_{\theta_1}^2 \frac{\partial^2 \dot{U}_o}{\partial x^2} + s_{\theta_1}^2 \frac{\partial^2 \dot{U}_o}{\partial y^2} + 2 s_{\theta_1} c_{\theta_1} \frac{\partial^2 \dot{U}_o}{\partial x \partial y} \right) \\ + \frac{L_2^2 \delta_{2b}^2}{2} \left(c_{\theta_2}^2 \frac{\partial^2 \dot{U}_o}{\partial x^2} + s_{\theta_2}^2 \frac{\partial^2 \dot{U}_o}{\partial y^2} + 2 s_{\theta_2} c_{\theta_2} \frac{\partial^2 \dot{U}_o}{\partial x \partial y} \right) \end{array} \right) \\ + N_E^2 \left(L_1 \delta_{1b} \left(c_{\theta_1} \frac{\partial \dot{U}_o}{\partial x} + s_{\theta_1} \frac{\partial \dot{U}_o}{\partial y} \right) + L_2 \delta_{2b} \left(c_{\theta_2} \frac{\partial \dot{U}_o}{\partial x} + s_{\theta_2} \frac{\partial \dot{U}_o}{\partial y} \right) \right) \end{array} \right) \\ + \varepsilon^2 \left(\begin{array}{l} T_E^2 \left(\begin{array}{l} \frac{L_1^2 \delta_{1b}^2}{2} \left(c_{\theta_1}^2 \frac{\partial^2 \dot{V}_o}{\partial x^2} + s_{\theta_1}^2 \frac{\partial^2 \dot{V}_o}{\partial y^2} + 2 s_{\theta_1} c_{\theta_1} \frac{\partial^2 \dot{V}_o}{\partial x \partial y} \right) \\ + \frac{L_2^2 \delta_{2b}^2}{2} \left(c_{\theta_2}^2 \frac{\partial^2 \dot{V}_o}{\partial x^2} + s_{\theta_2}^2 \frac{\partial^2 \dot{V}_o}{\partial y^2} + 2 s_{\theta_2} c_{\theta_2} \frac{\partial^2 \dot{V}_o}{\partial x \partial y} \right) \end{array} \right) \\ + N_E^2 \left(\begin{array}{l} \frac{L_1^2 \delta_{1b}^2}{2} \left(c_{\theta_1}^2 \frac{\partial^2 \dot{U}_o}{\partial x^2} + s_{\theta_1}^2 \frac{\partial^2 \dot{U}_o}{\partial y^2} + 2 s_{\theta_1} c_{\theta_1} \frac{\partial^2 \dot{U}_o}{\partial x \partial y} \right) \\ + \frac{L_2^2 \delta_{2b}^2}{2} \left(c_{\theta_2}^2 \frac{\partial^2 \dot{U}_o}{\partial x^2} + s_{\theta_2}^2 \frac{\partial^2 \dot{U}_o}{\partial y^2} + 2 s_{\theta_2} c_{\theta_2} \frac{\partial^2 \dot{U}_o}{\partial x \partial y} \right) \end{array} \right) \end{array} \right) \end{array} \right] \right] dV \qquad \text{(A.1)}$$

where $c_\theta, s_\theta, c_\theta^2$ and s_θ^2 denote $\cos\theta$, $\sin\theta$, $\cos^2\theta$ and$\sin^2\theta$; they are the components of the periodicity vectors [84].

Appendix B

Analytical derivation of the effective strain energy density

We present here an analytical method based on an evaluation at micro level of the strain energy density in order to compute the effective mechanical properties of a network materials.

One considers general 2D beam elements. The element kinematics is characterized by a displacement field $\mathbf{U}$ with displacement components u, v and rotation θ defined in the beam's local x, y frame, as depicted in Figure B.1.

Each beam works in tension-compression under the action of normal forces F_j^i and F_{j+1}^{i+1} applied to the extremity nodes and in flexion under the action of the transverse forces T_j^i, T_{j+1}^{i+1} and the moments M_j^i, M_{j+1}^{i+1}, as illustrated in Figure B.1.

We express the strain energy W_S generated by the element's nodal displacement and rotation as the sum of the extensional, flexural and shear energy contributions, as follows [84]:

$$W_S = \underbrace{\frac{1}{2}\frac{EA}{L}\left(u_{j+1}^{i+1} - u_j^i\right)^2}_{\text{Extension Energy}} + \underbrace{\frac{1}{2}\frac{EI}{L}\left(\theta_{j+1}^{i+1} - \theta_j^i\right)^2}_{\text{Flexion Energy}} + \underbrace{\frac{1}{2}\frac{12EI}{L^3}\left(\left(v_{j+1}^{i+1} - v_j^i\right) - \frac{L}{2}\left(\theta_{j+1}^{i+1} + \theta_j^i\right)\right)^2}_{\text{Shear Energy}} \qquad \text{(B.1)}$$

where E stands for the beam's material modulus, A for the beam's cross-sectional area, L for the beam's length, and I for the quadratic moment of the considered beam. The previously introduced parameters define the extensional EA/L, flexural EI/L, and shear rigidity $12EI/L^3$.

In order to take into account the surface effects, tensile, shear and flexural rigidities of the beam are modified as explained in Section 2:

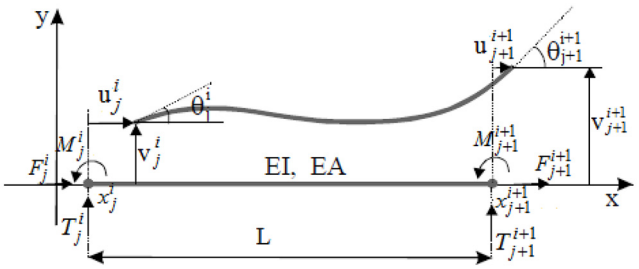

Figure B.1. Kinematics of a beam element.

$$\tilde{k}_l = \frac{\tilde{E}_B \tilde{A}}{l^b};\ \tilde{k}_c = \frac{12\tilde{E}_B \tilde{I}}{(l^b)^3};\ \tilde{k}_f = \frac{\tilde{E}_B \tilde{I}}{l^b}$$

such as $\tilde{E}_B = E_B(1 + \frac{l_s}{t})$

This entails the following modified expression of the strain energy:

$$W_S = \underbrace{\frac{1}{2}\tilde{k}_l\left(u_{j+1}^{i+1} - u_j^i\right)^2}_{\text{Extension Energy}} + \underbrace{\frac{1}{2}\tilde{k}_f\left(\theta_{j+1}^{i+1} - \theta_j^i\right)^2}_{\text{Flexion Energy}} + \underbrace{\frac{1}{2}\tilde{k}_c\left(\left(v_{j+1}^{i+1} - v_j^i\right) - \frac{L}{2}\left(\theta_{j+1}^{i+1} + \theta_j^i\right)\right)^2}_{\text{Shear Energy}} \tag{B.2}$$

We subsequently employ as a continuation method a Taylor expansion of the kinematic variables using a beam curvilinear coordinate s (for more details see Rahali et al. [84]), upon which we retrieve the following expressions for the beam's strain energy contributions in a continuum description:

$$W_{extension} = \frac{1}{2}\tilde{k}_l\left[L\frac{\partial u}{\partial s}\Big|_j^i + \frac{L^2}{2}\frac{\partial^2 u}{\partial s^2}\Big|_j^i\right]^2 = \frac{1}{2}\tilde{k}_l\left(\underbrace{\left(L\frac{\partial u}{\partial s}\Big|_j^i\right)^2}_{\text{Linear Energy}} + \underbrace{2\left(L\frac{\partial u}{\partial s}\Big|_j^i\right)\left(\frac{L^2}{2}\frac{\partial^2 u}{\partial s^2}\Big|_j^i\right)}_{\text{Coupling Energy}} + \underbrace{\left(\frac{L^2}{2}\frac{\partial^2 u}{\partial s^2}\Big|_j^i\right)^2}_{\text{SG Energy}}\right)$$

$$W_{flexion} = 0 \tag{B.3}$$

$$W_{shear} = \frac{1}{2}\tilde{k}_c\left[\left(L\frac{\partial v}{\partial s}\Big|_j^i + \frac{L^2}{2}\frac{\partial^2 v}{\partial s^2}\Big|_j^i\right) - \frac{L}{2}\left(2\frac{\partial v}{\partial s}\Big|_j^i\right)\right]^2 = \underbrace{\frac{1}{2}\tilde{k}_c\left[\left(\frac{L^2}{2}\frac{\partial^2 v}{\partial s^2}\Big|_j^i\right)\right]^2}_{\text{SG Energy}}$$

We note that the asymptotic development of equation (B.3) corresponds to the connection between two extremities nodes numbered as (i,j), $(i+1,j+1)$.Using the expressions in equation (B.3), we distinguish between energy contribution terms associated with the first-order gradient of the kinematic variables, coupling terms encompassing both first- and second-order derivatives and second gradient terms, defined exclusively through second-order derivatives of the kinematic variables. Naming the linear terms as W_{S_L}, the coupling terms as W_{S_C} and the second gradient terms as Ws_2, we define the total strain energy of the effective continuum as their sum:

$$W_S = W_{S_L} + W_{S_2} + W_{S_C} \tag{B.4}$$

The transition of the total energy expression, equation (B.4), is next made from the local curvilinear basis to the Cartesian global basis. The energy density is finally evaluated by dividing the total energy, elaborated as the sum of the energies of all beams comprising the unit cell in the Cartesian basis by the volume of the elementary unit cell. This methodology leads to the effective second gradient continuum replacing the initially discrete network. The Cauchy stress tensor σ_{ij} is defined by means of the first order

and coupling energy contributions while the hyperstress tensor S_{ijk} is elaborated from the second gradient and coupling energy terms as follows:

$$\sigma_{ij} = \frac{\partial(Ws_L + Ws_C)}{\partial\left(\partial u_i/\partial x_j\right)} \qquad S_{ijk} = \frac{\partial(Ws_2 + Ws_C)}{\partial\left(\partial^2 u_{ij}/\partial {x_k}^2\right)} \tag{B.5}$$

If we apply the previously elaborated methodology to the same square example presented in Section 3, the strain energy of the structure written as follows, in which indices k (in u_k, v_k, and θ_k) refer to the beam numbers:

$$W_s = W_{extension} + W_{flexion} + W_{shear} \tag{B.6}$$

with

$$W_{extension} = \begin{pmatrix} \frac{1}{2}\tilde{k}_{l_1}\left(u_1{}_{j+1}^{i-1} - u_1{}_{j-1}^{i-1}\right)^2 + \frac{1}{2}\tilde{k}_{l_2}\left(u_2{}_{j+2}^{i-1} - u_2{}_{j+1}^{i-1}\right)^2 + \frac{1}{2}\tilde{k}_{l_3}\left(u_3{}_{j-1}^{i+1} - u_3{}_{j-1}^{i-1}\right)^2 + \frac{1}{2}\tilde{k}_{l_4}\left(u_4{}_{j-1}^{i+2} - u_4{}_{j-1}^{i+1}\right)^2 \\ + \frac{1}{2}\tilde{k}_{l_5}\left(u_5{}_{j}^{i} - u_5{}_{j-1}^{i-1}\right)^2 + \frac{1}{2}\tilde{k}_{l_6}\left(u_6{}_{j+2}^{i+2} - u_6{}_{j}^{i}\right)^2 + \frac{1}{2}\tilde{k}_{l_7}\left(u_7{}_{j}^{i} - u_7{}_{j-1}^{i+1}\right)^2 + \frac{1}{2}\tilde{k}_{l_8}\left(u_8{}_{j+1}^{i-1} - u_8{}_{j}^{i}\right)^2 \end{pmatrix}$$

$$W_{flexion} = \begin{pmatrix} \frac{1}{2}\tilde{k}_{f_1}\left(\theta_1{}_{j+1}^{i-1} - \theta_1{}_{j-1}^{i-1}\right)^2 + \frac{1}{2}\tilde{k}_{f_2}\left(\theta_2{}_{j+2}^{i-1} - \theta_2{}_{j+1}^{i-1}\right)^2 + \frac{1}{2}\tilde{k}_{f_3}\left(\theta_3{}_{j-1}^{i+1} - \theta_3{}_{j-1}^{i-1}\right)^2 + \frac{1}{2}\tilde{k}_{f_4}\left(\theta_4{}_{j-1}^{i+2} - \theta_4{}_{j-1}^{i+1}\right)^2 \\ + \frac{1}{2}\tilde{k}_{f_5}\left(\theta_5{}_{j}^{i} - \theta_5{}_{j-1}^{i-1}\right)^2 + \frac{1}{2}\tilde{k}_{f_6}\left(\theta_6{}_{j+2}^{i+2} - \theta_6{}_{j}^{i}\right)^2 + \frac{1}{2}\tilde{k}_{f_7}\left(\theta_7{}_{j}^{i} - \theta_7{}_{j-1}^{i+1}\right)^2 + \frac{1}{2}\tilde{k}_{f_8}\left(\theta_8{}_{j+1}^{i-1} - \theta_8{}_{j}^{i}\right)^2 \end{pmatrix} = 0$$

and

$$W_{shear} = \begin{pmatrix} \frac{1}{2}\tilde{k}_{c_1}\left(\left(v_1{}_{j+1}^{i-1} - v_1{}_{j-1}^{i-1}\right) - \frac{L}{4}\left(\theta_1{}_{j+1}^{i-1} + \theta_1{}_{j-1}^{i-1}\right)\right)^2 + \frac{1}{2}\tilde{k}_{c_2}\left(\left(v_2{}_{j+2}^{i-1} - v_2{}_{j+1}^{i-1}\right) - \frac{L}{4}\left(\theta_2{}_{j+1}^{i+1} + \theta_2{}_{j+1}^{i-1}\right)\right)^2 \\ + \frac{1}{2}\tilde{k}_{c_3}\left(\left(v_3{}_{j-1}^{i+1} - v_3{}_{j-1}^{i-1}\right) - \frac{L}{4}\left(\theta_3{}_{j-1}^{i+1} + \theta_3{}_{j-1}^{i-1}\right)\right)^2 + \frac{1}{2}\tilde{k}_{c_4}\left(\left(v_4{}_{j-1}^{i+2} - v_4{}_{j-1}^{i+1}\right) - \frac{L}{4}\left(\theta_4{}_{j-1}^{i+2} + \theta_4{}_{j-1}^{i+1}\right)\right)^2 \\ + \frac{1}{2}\tilde{k}_{c_5}\left(\left(v_5{}_{j}^{i} - v_5{}_{j-1}^{i-1}\right) - \frac{L}{4\sqrt{2}}\left(\theta_5{}_{j}^{i} + \theta_5{}_{j-1}^{i-1}\right)\right)^2 + \frac{1}{2}\tilde{k}_{c_6}\left(\left(v_6{}_{j+2}^{i+2} - v_6{}_{j}^{i}\right) - \frac{3\sqrt{2}L}{8}\left(\theta_6{}_{j+2}^{i+2} + \theta_6{}_{j}^{i}\right)\right)^2 \\ + \frac{1}{2}\tilde{k}_{c_7}\left(\left(v_7{}_{j}^{i} - v_7{}_{j-1}^{i+1}\right) - \frac{L}{4\sqrt{2}}\left(\theta_7{}_{j}^{i} + \theta_7{}_{j-1}^{i+1}\right)\right)^2 + \frac{1}{2}\tilde{k}_{c_8}\left(\left(v_8{}_{j+1}^{i-1} - v_8{}_{j}^{i}\right) - \frac{L}{4\sqrt{2}}\left(\theta_8{}_{j+1}^{i-1} + \theta_8{}_{j}^{i}\right)\right)^2 \end{pmatrix}$$

We use the Bernoulli model including a local rotation, in addition to the displacement acting as the translational degree of freedom. The rotation is here limited to the zero order (one order less than the displacement), which entails the following relations:

$$\theta_{j+1}^{i+1} = \theta_{j-1}^{i-1} = \theta_j^i = \left.\frac{\partial v}{\partial s}\right|_j^i \ ;$$

After some developments and simplifications (we refer the reader to Rahali et al. [84] for more details related to the different steps of the method), one can compute the energy density by dividing by the area of the elementary unit cell, i.e. $S = L^2$, viz.

$$W^* = W_s/S = \frac{1}{L^2}\left(W_{extension} + W_{shear}\right) \tag{B.7}$$

This allows us to compute the effective second gradient continuum properties. One can therefore deduce the Cauchy stress tensor σ_{ij} and the hyperstress tensor S_{ijk}.